11

Photonic Crystal Coupled to N-V Center in Diamond

Luca Marseglia
Centre for Quantum Photonics, H. H. Wills Physics Laboratory & Department of Electrical and Electronic Engineering, University of Bristol, BS8 1UB United Kingdom

1. Introduction

In this work we aim to exploit one of the most studied defect color centers in diamond , the negatively charged nitrogen vacancy (NV^-) color center, a three level system which emits a single photon at a wavelength of $637nm$ providing a possible deterministic single photon emitter very useful for quantum computing applications. Moreover the possibility of placing a NV^- in a photonic crystal cavity will enhance the coupling between photons and NV^- center. This could also allow us to address the ground state of the NV^- center, whose spin, could be used as qubit. It is also remarkable to notice that for quantum computing purposes it is very useful to increase the light collection from the NV^- centers, and in order to do that we performed a study of another structure, the solid immersion lens, which consists of an hemisphere whose center is at the position of an emitter, in this case the NV^- center, increasing the collection of the light from it. In order to create these structures we used a method called focused ion beam which allowed us to etch directly into the diamond many different kinds of structures. In order to allow an interaction between these structures and the NV^- centers we need to have a method to locate the NV^- center precisely under the etched structures. We developed a new technique (Marseglia et al. (2011)) where we show how to mark a single NV^- center and how to etch a desired structure over it on demand. This technique gave very good results allowing us to etch a solid immersion lens onto a NV^- previously located and characterized, increasing the light collection from the NV^- of a factor of $8\times$.

2. Introduction to Nitrogen Vacancy center in diamond

Diamond has emerged in recent years as a promising platform for quantum communication and spin qubit operations as shown by Gabel et al. (2006), as well as for “quantum imaging" based on single spin magnetic resonance or nanoscopy. Impressive demonstrations in all these areas have mostly been based on the negatively-charged nitrogen vacancy center, NV^-, which consists of a substitutional nitrogen atom adjacent to a carbon vacancy. Due to its useful optical and magnetic spin selection properties, the NV^- center has been used by Kurtsiefer et al. (2000) to demonstrate a stable single photon source and single spin manipulations (Hanson et al. (2006)) at room temperature. A single-photon source based on NV^- in nano-diamond is already commercially available, and a ground state spin coherence time of $15ms$ has been observed in ultra-pure diamond at room temperature. At present, one of the biggest issues preventing diamond from taking the lead among competing technologies

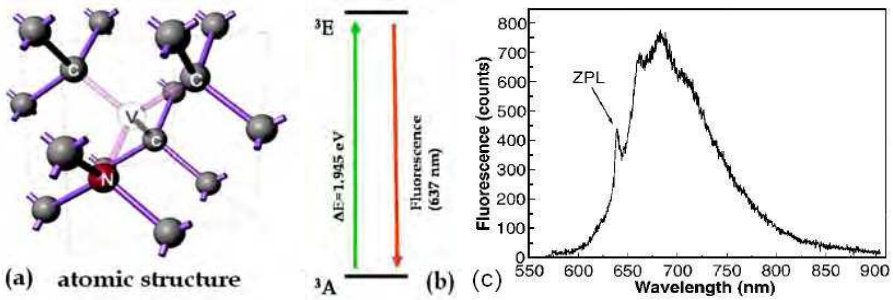

Fig. 1. a)Atomic structure of NV^- center in diamond(N=nitrogen V=Vacancy, C=Carbon) b) Energy level scheme of NV^- center. c) Fluorescence spectrum of a single NV^- defect center. The wavelength of the zero phonon line (ZPL) is $637nm$ ($1.945eV$). Excitation was at $514nm$ (Image taken from Gruber et al. (1997))

is the difficulty in fabricating photonic devices to couple and guide light. For the realization of large-scale quantum information processing protocols (e.g. via photonic module approaches) or for quantum repeater systems, it will be necessary to connect NV^- centers through "flying" qubits such as photons. To achieve this, micro-cavities and waveguides are needed to enable the transfer of quantum information between the electron spin of the NV^- center and a photon. In this work I will show some applications of diamond useful for quantum computing. Synthetic diamonds can be doped in order to create implanted NV^- center which interacts with light, as described further. From its discovery, it has not been very clear if the NV^- were a proper two level system. Recently it has been shown that it has properties more typical of a three level system with a metastable level. In its ground state it has spin $s = 1$ and different emission rates for transitions to the ground states, so NV^- center can be also exploited in order to achieve spin readout.

3. Interaction of N-V center with light

The NV^- center in diamond occurs naturally or is produced after radiation damage and annealing in vacuum. As described earlier is made by substitutional nitrogen atom adjacent to a vacancy in carbon lattice in the diamond as depicted in Fig.1a. The NV^- center has attracted a lot of interest because it can be optically addressed as a single quantum system as discussed by van Oortt et al. (1988). The NV^- center behaves as a two level system with a transition from the excited state to the ground state providing a single photon of $637nm$, as shown in Fig.1b. This is a very useful characteristic for quantum information purposes because it can be used as single photon source. Let us remember that a characteristic of the NV^- center is a zero-phonon line (ZPL), in the spectrum at room temperature, at $637nm$ as shown in Fig.1c, the zero-phonon line constitutes the line shape of individual light absorbing and emitting molecules embedded into the crystal lattice. The state of NV^- center ground state spin strongly modulates the rate of spontaneous emission from the ${}^3E \leftrightarrow {}^3A$ sub-levels providing a mechanism for spin read out as discussed by Hanson et al. (2006). We have recently shown theoretically (Young et al. (2009)) that spin readout with a small number of photons could be achieved by placing the NV^- centre in a subwavelength scale micro-cavity with a moderate Q-factor($Q \sim 3000$). So one of our aims is to optimize the output coupling of photons from diamond color centers into waveguides and free space to

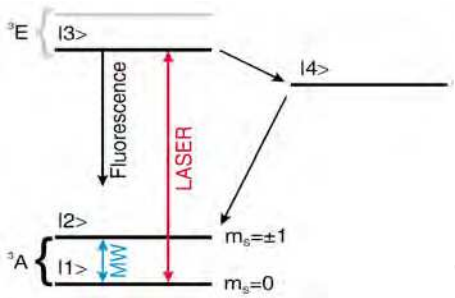

Fig. 2. Energy level scheme of the nitrogen vacancy defect center in diamond. The greyed out lines correspond to the $m_s = \pm 1$ sublevels (Image taken from Jelezko et al. (2004b))

increase the efficiency of single photon sources and to enable faster single spin read-out. In order to do that we want to study resonant structures. These structures confine the light close to the emitter allowing cavity-QED effects to be exploited to direct an emitted photon into a particular spatial mode and will allow us to enhance the ZPL. An improvement of the photon emission rate and photon indistinguishability for NV^-can be achieved due to the (coherent) interaction with the highly localized photon field of the cavity. In principle a high-Q micro-cavity can be realized directly in diamond but the first experimental demonstrations with micro-disk resonators and photonic crystal cavities, made for example by Wang et al. (2007), suffered from large scattering losses due to the poly-crystalline nature of the diamond material used. The fabrication of high-Q cavities in single crystal diamond is very challenging because vertical optical confinement within diamond requires either a $3D$ etching process or a method for fabricating thin single crystal diamond films. We want analyze photonic crystal structures in diamond and fabrication methods to achieve efficient spin read-out in low-Q cavities. Electronic spin resonance (ESR) experiments performed by Jelezko et al. (2004a) has shown that the electronic ground state of NV^-center (^3A) is paramagnetic. Indeed the electronic ground state of the NV^-center is a spin triplet that exhibits a $2.87GHz$ zero-field splitting defining the z axis of the electron spin. An application of a small magnetic field splits the magnetic sublevel $m_s = \pm 1$ energy level structure of the NV^-center, as we can see in Fig.2. Electron spin relaxation times (T_1) of defect centers in diamond range from millisecond at room temperature to seconds at low temperature. Several experiments have shown the manipulation of the ground state spin of a NV^-center using optically detected magnetic resonance (ODMR) techniques, the main problem in using ODMR is that detection step involves observing fluorescence cycles from the NV^-center which has a probability of destroying the spin. Another characteristic of NV^-center useful for quantum information storage is the capability of transferring its electronic spin state to nuclear spins. Experiments performed by van Oortt et al. (1988) have shown the possibility of manipulating nuclear spins of NV^-. Nuclear spins are of fundamental importance for storage and processing of quantum information, their excellent coherence properties make them a superior qubit candidate even at room temperature.

4. Beyond the two level system model

In order to study the dynamics of the NV^-center, remembering that $m_e << m_C$ where m_e is the value of the mass of the electrons and m_C is the value of the mass of carbon atom,

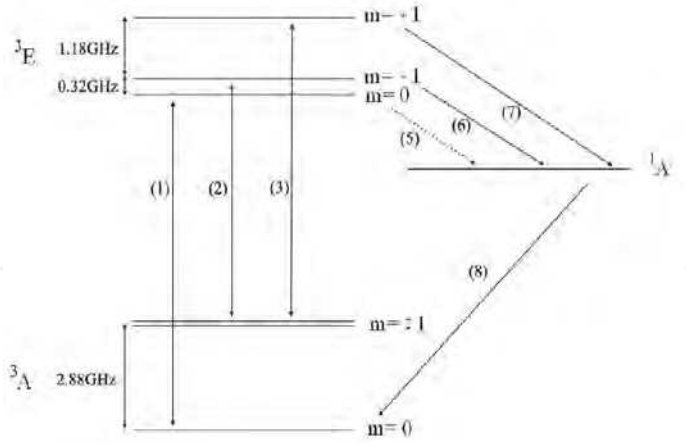

Fig. 3. Experimentally measured energy level diagram of the NV center in diamond showing the experimentally determined ground and excited state splitting. The defect has zero phonon line at 637 nm, with width of order MHz at low temperatures (image taken from Young et al. (2009)).

we make the so called Born-Oppenheimer approximation, in which we consider the nuclei fixed in a crystal geometry and the coordinates of the electrons are considered with respect to them. When a defect is present it breaks down the crystal symmetry and, regarding the NV^-center, we have a contribution of one electron from each carbon atom, the nitrogen contributes two electrons, and an extra electron comes from the environment as described by Gali et al. (2008), possibly given by substitutional nitrogen, so ending with a total number of six electrons. The excited level of the $NV^-$is not yet very well understood explicitly but there are many theoretical descriptions using group theory and partially confirmed by experimental results. The joint use of group theory and numerical calculations has led to predictions of the ordering of the levels of the ground state and excited states of the NV^-. Taking account the coulomb interaction, spin-orbit effect and spin-spin coupling it explains the splitting of the levels initially degenerate giving rise to different transition between them. Without entering in to detailed group theory calculations we can summarize by stating that the hamiltonian of the system is composed of three elements, the coulomb interaction H_C, the spin orbit interaction H_{SO} and the spin-spin interaction H_{SS}.

$$H = H_C + H_{SO} + H_{SS} \tag{1}$$

The dynamics of the system is resolved by solving the hamiltonian in free space with coulomb interaction as potential and the spin-orbit and spin-spin interaction were eventually added as perturbations. We show the detailed energy level structure of the NV^-center in Fig.3. The overall effect can be summarized as follows, the coulomb interaction, splits the degeneracy between singlet and triplets of the ground state and the first excited state, the spin orbit interaction splits the states which have $M_{s=0}$ and $M_{s=\pm1}$ and finally the spin-spin splits the A levels. The end result is that the optical transitions between ground and excited states $(1-3)$ occur at different energies. In the absence of external fields the ground state is a spin triplet split by 2.88 GHz due to spin$-$spin interactions. Manson et al. (2006) showed that the excited state is a triplet split by spin-spin interactions, but with the further addition of spin-orbit

coupling . Recent experimental evidence performed by Tamarat et al. (2008), has uncovered this excited state structure (Fig.3). The net effect of spin-spin and spin-orbit interactions is to create a detuning $\approx$ 1.4 GHz (6μeV) between the transitions ${}^3A_{(m=0)} \rightarrow {}^3E_{(m=0)}$ (transitions 1)and ${}^3A_{(m=+1)} \rightarrow {}^3E_{(m=+1)}$ (transition 3). A similar detuning of $\approx$ 2.5 GHz (10μeV) exists for the ${}^3A_{(m=-1)} \rightarrow {}^3E_{(m=-1)}$ (transition 2), the rates for these three transition is $k_1 = k_2 = k_3 = 77MHz$ which gives a spontaneous emission (SE) lifetime $\tau \approx 13ns$. The energy level structure is not simply a ground and excited triplet state, there also exists an intermediate singlet state ${}^1A$ arising from Coulomb interactions. There is a probability of the transition ${}^3E \rightarrow {}^1A$, with different rates depending on the spin. For the ${}^3E_{m=\pm1}$ states (transitions 6,7) both theoretical predictions and experimental results suggest that the decay rate is around $k_6 = k_7 = 30MHz$ giving a spontaneous emission (SE) lifetime $\tau \approx 30ns$. For the ${}^3E_{m=0}$ state (transition 5) theoretically the rate of decay to the singlet should be zero, however, experimental observations made by Jelezko & Wrachtrup (2004) have shown the rate to be $\approx 10^{-4} \times 1/\tau$. Since the ${}^1A$ singlet state decays preferentially to the ${}^3E_{m=0}$ state (transition 8), then it is clear from the rates above that broadband excitation leads to spin polarization in the spin zero ground state. Since transition 8 is non-radiative then there will be a dark period in the fluorescence when ${}^1A$ becomes populated, and as the decay rate from ${}^3E_{m=\pm1}$, $k_8 = 3.3MHz$, to the singlet state is much larger than from ${}^3E_{m=0}$, the change in intensity measures the spin state. Clearly using fluorescence intensity to detect the spin state has a probability to flip the spin, therefore it would seem necessary for a scheme to suppress this. However, spin-flip transitions are essential to initialize the system. Thus a compromise is required between the perfectly cyclic spin preserving transitions required for readout and the spin flip transitions needed for reset.

5. Photonic crystals

To take advantage of atom-photon coupling using NV^-, as required by many quantum protocols, cavity structures are required. Again, concentrating on monolithic diamond solutions, photonic crystal cavities are the most natural structures to explore. A photonic crystal structure modulates the propagation of light in a way that is analogous to the way a semiconductor crystal modulates the motion of electrons. In both cases a periodic structure gives rise to 'band-gap' behavior, with a photon (electron) being allowed or not allowed to propagate depending on its wave vector. In photonic crystals the periodicity is comprised of regions of higher and lower dielectric constants. The basic physical phenomenon is based on diffraction, the period needs to be of the order of a half-wavelength of the light to be confined. For visible light the wavelength goes from 200nm (blue) to 650nm (red), leading to a real challenge in order to make the fabrication of optical photonic crystals because of the small dimensions. Breaking the periodicity in a controlled way creates nanocavities that confine light to extremely small volumes in which the lightmatter interaction is dominated by cavity quantum electrodynamic. We have previously described the characteristics of the NV^-center, a three level system which is promising as an efficient room temperature source of single photons at a wavelength of 637nm. We pointed out that the NV^-center looks very promising for performing quantum spin readout, which is also useful for quantum computing purposes. Zero-phonon emission, at 637nm, accounts for only a small fraction ($\sim$ 4%) of NV^-fluorescence, with the majority of emitted photons falling in the very broad ($\sim$ 200nm) phonon-assisted sideband. By coupling the NV^-center to a photonic crystal cavity, spontaneous emission in the phonon sideband can be suppressed and emission in

the zero-phonon line can be enhanced (Su et al. (2008)) so the photonic crystals offers a controllable electromagnetic environment, ideal for the compact integration and isolation of the fragile quantum system. The challenges of engineering the parameters of the photonic crystal in diamond at this scale are not trivial, as described further where we will show how to tune a cavity to increase the efficiency of light collection from an emitter placed in it. Indeed, a single photon emitted by a NV^-could then interact with another NV^-allowing entanglement between both qubits represented by the spin of the NV^-centers ase described by Neumann et al. (2008). High-Q resonators of different kinds have been fabricated in non-diamond materials and coupled to NV^-emission from nano-diamonds. Since we are concerned here with developing monolithic photonics, it is necessary to fabricate cavities in the diamond itself. It should be noted that photonic crystal cavities have been fabricated in diamond films and an un-coupled Q-factor as high as 585 at $637nm$ has been measured by Wang et al. (2007). The polycrystal nature of the material used in those demonstrations makes it unsuitable for our purposes due to enhanced scattering and background fluorescence. We aim to fabricate photonic crystal cavities in ultra-high-purity type IIa single-crystal diamond (Element Six) grown by chemical vapor deposition. This material has extremely low levels of nitrogen (less than $1ppb$), and very few native NV^-centers, making it the ideal material for creating NV^-centers in a controlled fashion by implantation and annealing. In order to have strong coupling we need to have a cavity with high Q factor and small modal volume, but a cavity with a more moderate Q would still be useful. In particular, a scheme for reading out the ground state spin of an NV^-center has been described by our group (Young et al. (2009)), that requires a Q (before coupling) of only ~ 3000. This scheme exploits the zero-field splitting in the NV^-center ground state and uses narrow band resonant excitation to achieve high-fidelity read-out of the ground state spin with just a few excitation cycles.

6. Crystals geometry

A rigid body is called symmetric if it remains identical to itself after a translation, a rotation or a reflection, which are called the symmetrical operations of the body. A composition of two symmetrical operations is still a symmetrical operation and every symmetrical operation has got its own inverse which is still a symmetrical operation, so all the operations which satisfies these requirements form a set. The general element of this set can be described by a matrix transformation in cartesian coordinates as follows

$$\begin{pmatrix} x'_1 \\ x'_2 \\ x'_3 \end{pmatrix} = \begin{pmatrix} \alpha_{11} & \alpha_{12} & \alpha_{13} \\ \alpha_{21} & \alpha_{22} & \alpha_{23} \\ \alpha_{31} & \alpha_{32} & \alpha_{33} \end{pmatrix} \begin{pmatrix} x_1 \\ x_2 \\ x_3 \end{pmatrix} + \begin{pmatrix} a_1 \\ a_2 \\ a_3 \end{pmatrix} \tag{2}$$

the choice of the parameters lead to interesting subsets as for example if we choose all the value $a_i = 0$ we have the so called point sets. if we choose the α matrix as unitary

$$\alpha = \begin{pmatrix} 1 & 0 & 0 \\ 0 & 1 & 0 \\ 0 & 0 & 1 \end{pmatrix} \tag{3}$$

we have the translations set which we will focus on. The crystal contains a lattice of equivalent points known as *Bravais Lattice*, a mathematical entity defined as the set of points which looks

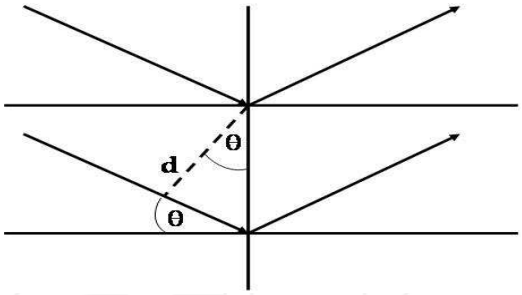

Fig. 4. Bragg Hypothesis

always the same after any translations between the points on the Bravais lattice itself so, for example if a translational vector $\overrightarrow{\mathbf{R}}$ connects two points of the set, an integer application of the the same vector can connect any point of the Bravais lattice to the appropriate point of itself. A *Crystal Lattice* is obtained if a simple structure, called the base, is repeated in space in order to create a Bravais lattice, which can be seen as a way of locating identical copies of the base in the space. In a physical crystal the base is made by set of atoms or ions called the unit cell. It is possible to generate the whole set of points of a Bravais lattice with three primitive vectors. All the translations are linear combinations of these three vectors

$$\overrightarrow{\mathbf{R}} = n\overrightarrow{\mathbf{a}}_1 + m\overrightarrow{\mathbf{a}}_2 + p\overrightarrow{\mathbf{a}}_3 \tag{4}$$

with n, m, p integers. The solid made by the three primitive vectors is called a primitive cell, which has the lattice points at its vertices. The repetition of the primitive cell gives rise to the crystal lattice.

7. Bragg scattering

If we want to study the scattering of the light incident on a crystal lattice we shall start from the Bragg approximation, in which the crystal is considered to be made from lattice planes. The light is incident on these planes with angle of incidence θ. The underlying hypothesis is that each plane partially reflects the light. If **d** (Fig.4) is the distance between a pair of planes the constructive interference condition between the reflected rays is

$$2d\sin\theta = n\lambda \tag{5}$$

where λ is the wavelength and n is an integer. We now generalize this principle to the scattering of light from a three dimensional crystal following. Let's suppose a monochromatic wave of wave vector $\overrightarrow{k}$ and angular frequency ω hits the crystal with amplitude

$$\mathbf{F}(\overrightarrow{x}) = \mathbf{F_0} exp(i(\overrightarrow{k} \cdot \overrightarrow{x} - \omega t)) \tag{6}$$

If $\overrightarrow{\mathbf{R}}$ is the position of an atom in the lattice the amplitude of the wavelength incident on it at $t = 0$ is

$$\mathbf{F}(\overrightarrow{\mathbf{R}}) = \mathbf{F_0} exp(i\overrightarrow{k} \cdot \overrightarrow{\mathbf{R}}) \tag{7}$$

So the wave spread by the atom is a spherical wave which has amplitude at a point $\overrightarrow{\rho}$ given by $exp(ikr)/r$, where $\overrightarrow{r} = \overrightarrow{\rho} - \overrightarrow{\mathbf{R}}$. The whole amplitude is given by

$$exp(i\overrightarrow{k} \cdot \overrightarrow{\mathbf{R}}) \cdot exp(ikr)/r \simeq exp(i\overrightarrow{k} \cdot \overrightarrow{\mathbf{R}} + ikr)/\rho \tag{8}$$

If we choose the origin of the crystal and suppose that the position $\overrightarrow{\rho}$ in which we are looking the wave is far from the the crystal so that $r \simeq \rho$ and if θ is the angle between $\overrightarrow{\rho}$ and $\overrightarrow{\mathbf{R}}$. Then we can say that:

$$r^2 = (\overrightarrow{\rho} - \overrightarrow{\mathbf{R}})^2 = \rho^2 + R^2 - 2\rho R cos\theta \tag{9}$$

$$r = \rho\sqrt{1 - 2\frac{R}{\rho}cos\theta + \frac{R^2}{\rho^2}} \simeq \rho - Rcos\theta \tag{10}$$

and the amplitude of the wave is determined by the phase factor.

$$exp(i\overrightarrow{k} \cdot \overrightarrow{\mathbf{R}} + ik\rho - ikRcos\theta) = exp(ik\rho)exp(i\overrightarrow{k}\overrightarrow{\mathbf{R}} - ikRcos\theta) \tag{11}$$

At great distance from the source the spherical wave can be considered to be a plane wave with $\overrightarrow{k'} = \overrightarrow{k}cos\theta$ as wave vector with the same modulus of the of the incident wave, propagating in a direction which forms an angle θ respect to $\overrightarrow{\mathbf{R}}$ so with value ρ and with the amplitude depending by the position of the atom as

$$exp(-i\Delta\overrightarrow{k} \cdot \overrightarrow{\mathbf{R}}) \tag{12}$$

with

$$\Delta\overrightarrow{k} = \overrightarrow{k'} - \overrightarrow{k} \tag{13}$$

If $\overrightarrow{a}$, $\overrightarrow{b}$ and $\overrightarrow{c}$ are the primitive vectors of the Bravais lattice so we can say

$$R = m\overrightarrow{a} + n\overrightarrow{b} + p\overrightarrow{c} \tag{14}$$

where m,n and p are integers. Let's suppose these three numbers can vary between 0 and $M-1$ so the crystals contains M^3 primitive cells. The total amplitude in the position ρ will be proportional to

$$A \equiv \sum_{\overrightarrow{R}} exp(-i\Delta\overrightarrow{k} \cdot \overrightarrow{\mathbf{R}}) = \sum_{nmp} exp[-i(m\overrightarrow{a} + n\overrightarrow{b} + p\overrightarrow{c}) \cdot \Delta\overrightarrow{k}] =$$
$$(\sum_m exp[-im(\overrightarrow{a} \cdot \Delta\overrightarrow{k})])(\sum_n exp[-in(\overrightarrow{b} \cdot \Delta\overrightarrow{k})])(\sum_p exp[-ip(\overrightarrow{c} \cdot \Delta\overrightarrow{k})]) \tag{15}$$

so the intensity is given by

$$|\mathbf{A}|^2 = |\sum_m exp[-im(\overrightarrow{a} \cdot \Delta\overrightarrow{k})]|^2|...|^2|...|^2 \tag{16}$$

any of these value can be computed using the geometrical series and multiplying by the complex conjugate we can show that

$$|\sum_m exp(-im(\overrightarrow{a} \cdot \Delta\overrightarrow{k}))|^2 = \frac{\sin^2\frac{1}{2}M(\overrightarrow{a} \cdot \Delta\overrightarrow{k})}{\sin^2\frac{1}{2}(\overrightarrow{a} \cdot \Delta\overrightarrow{k})} \tag{17}$$

This function of $\overrightarrow{a} \cdot \Delta \overrightarrow{k}$ is a peak function which has the absolute maximum values at

$$\overrightarrow{a} \cdot \Delta \overrightarrow{k} = 2\pi q \tag{18}$$

where q is an integer number, which gives the equation 17 the value of $\mathbf{M}^2$. The width of these maximum values is measured from the consequent zeros which are at

$$\overrightarrow{a} \cdot \Delta \overrightarrow{k} = 2\pi q + \epsilon \tag{19}$$

where ϵ is the smallest number different from zero so that

$$\sin(\frac{1}{2}M\epsilon) = 0 \tag{20}$$

giving us

$$\frac{1}{2}\mathbf{M}\epsilon = \pi \tag{21}$$

$$\epsilon = \frac{2\pi}{\mathbf{M}} \tag{22}$$

So the width of the maximum is proportional to $\frac{1}{M}$ and the area of the peak is given by the height ($\propto M^2$) times the width ($\propto \frac{1}{M}$) so it's proportional to the number $\mathbf{M}$ of atoms present in the line where the $\overrightarrow{a}$ vector lies. So taking all of equation 16 we see that when the crystal contains M^3 atoms the peaks of the scattered intensity will be proportional to M^3. They appear in the direction which satisfies simultaneously the three **Laue equations** as we see

$$\overrightarrow{a} \cdot \Delta \overrightarrow{k} = 2\pi q;\ \overrightarrow{b} \cdot \Delta \overrightarrow{k} = 2\pi r;\ \overrightarrow{c} \cdot \Delta \overrightarrow{k} = 2\pi s \tag{23}$$

where q,r and s are three integer numbers. The Laue Equation can be easily solved rewriting $\Delta \overrightarrow{k}$ as linear combination of multiple integers of three vectors $\overrightarrow{\mathbf{A}}$, $\overrightarrow{\mathbf{B}}$ and $\overrightarrow{\mathbf{C}}$

$$\Delta \overrightarrow{k} = q\overrightarrow{\mathbf{A}} + r\overrightarrow{\mathbf{B}} + s\overrightarrow{\mathbf{C}} \tag{24}$$

so that

$$\begin{aligned} &\overrightarrow{\mathbf{A}} \cdot \overrightarrow{a} = 2\pi, \quad \overrightarrow{\mathbf{B}} \cdot \overrightarrow{a} = 0, \quad \overrightarrow{\mathbf{C}} \cdot \overrightarrow{a} = 0, \\ &\overrightarrow{\mathbf{A}} \cdot \overrightarrow{b} = 0, \quad \overrightarrow{\mathbf{B}} \cdot \overrightarrow{b} = 2\pi, \quad \overrightarrow{\mathbf{C}} \cdot \overrightarrow{c} = 0, \\ &\overrightarrow{\mathbf{A}} \cdot \overrightarrow{c} = 0, \quad \overrightarrow{\mathbf{B}} \cdot \overrightarrow{c} = 0, \quad \overrightarrow{\mathbf{C}} \cdot \overrightarrow{c} = 2\pi, \end{aligned} \tag{25}$$

where the $\overrightarrow{\mathbf{A}}$ vector is perpendicular to the plane made by $\overrightarrow{b}, \overrightarrow{c}$, the vector $\overrightarrow{\mathbf{B}}$ is perpendicular to the plane made by $\overrightarrow{a}, \overrightarrow{c}$ and the $\overrightarrow{\mathbf{C}}$ vector is perpendicular to the plane made by $\overrightarrow{a}, \overrightarrow{b}$. The equations in 25 can be all satisfied choosing

$$\overrightarrow{\mathbf{A}} = 2\pi \frac{\overrightarrow{b} \times \overrightarrow{c}}{\overrightarrow{a} \cdot b \times \overrightarrow{c}};\ \overrightarrow{\mathbf{B}} = 2\pi \frac{\overrightarrow{c} \times \overrightarrow{a}}{\overrightarrow{a} \cdot b \times \overrightarrow{c}};\ \overrightarrow{\mathbf{C}} = 2\pi \frac{\overrightarrow{a} \times \overrightarrow{b}}{\overrightarrow{a} \cdot b \times \overrightarrow{c}} \tag{26}$$

these are the primitive vectors of a new lattice called the **reciprocal lattice**. For any crystal lattice in the real world, which will be called the direct lattice, we can consider a corresponding mathematical entity called the reciprocal lattice. The translation vectors of the crystal lattice

have the dimension of a length [L], the ones of the reciprocal lattice have the dimension of a $[L]^{-1}$. If we consider a function which has the spatial periodicity of the lattice

$$f(\overrightarrow{r}) = f(\overrightarrow{r} + \overrightarrow{\mathbf{R}}) \; with \;\; \overrightarrow{\mathbf{R}} = n\overrightarrow{a} + m\overrightarrow{b} + p\overrightarrow{c} \tag{27}$$

it can be represented by the Fourier Series

$$f(\overrightarrow{r}) = \sum_{\overrightarrow{k}} \widetilde{f}(\overrightarrow{k}) exp(i\overrightarrow{k} \cdot \overrightarrow{r}) \tag{28}$$

and the only vectors in the sum are the translational vectors of the reciprocal lattice

$$\overrightarrow{\mathbf{G}} = h\overrightarrow{\mathbf{A}} + k\overrightarrow{\mathbf{B}} + l\overrightarrow{\mathbf{C}} \tag{29}$$

with

$$e^{i\overrightarrow{\mathbf{G}} \cdot \overrightarrow{\mathbf{R}}} = 1 \tag{30}$$

because

$$\overrightarrow{\mathbf{G}} \cdot \overrightarrow{\mathbf{R}} = 2\pi(hm + kn + lp) = 2n\pi \tag{31}$$

where n is an integer, so the reciprocal lattice is the Fourier transform of the direct lattice. It is very important to note that every translational vector is perpendicular to a lattice plane of the direct lattice. So let's consider a translational vector of the reciprocal lattice,

$$\overrightarrow{\mathbf{G}} = h\overrightarrow{\mathbf{A}} + k\overrightarrow{\mathbf{B}} + l\overrightarrow{\mathbf{C}} \tag{32}$$

and let m,n and p be three integers obtained considering the greatest common divisor $\mathfrak{D}$ of h,k,and l and dividing by h,k,and l. So the three numbers m,n and p define the lattice plane which intersects the line $\overrightarrow{a}$ in the point $m\overrightarrow{a}$, the line $\overrightarrow{b}$ in the point $n\overrightarrow{b}$ and the the line $\overrightarrow{c}$ in the point $p\overrightarrow{c}$. The vectors $m\overrightarrow{a} - n\overrightarrow{b}$, $m\overrightarrow{a} - p\overrightarrow{c}$ and $n\overrightarrow{b} - p\overrightarrow{c}$ lie on the same plane and are perpendicular to $\overrightarrow{\mathbf{G}}$. Indeed

$$\begin{aligned} \overrightarrow{\mathbf{G}} \cdot (m\overrightarrow{a} - n\overrightarrow{b}) &= 2\pi(mh - nk) = 0 \\ \overrightarrow{\mathbf{G}} \cdot (m\overrightarrow{a} - p\overrightarrow{c}) &= 2\pi(mh - pl) = 0 \\ \overrightarrow{\mathbf{G}} \cdot (n\overrightarrow{b} - p\overrightarrow{c}) &= 2\pi(nk - pl) = 0 \end{aligned} \tag{33}$$

because by construction

$$m = \frac{\mathfrak{D}}{h}; n = \frac{\mathfrak{D}}{k}; p = \frac{\mathfrak{D}}{l}; \tag{34}$$

and so

$$\begin{aligned} mh - nk &= \mathfrak{D} - \mathfrak{D} = 0 \\ mh - pl &= \mathfrak{D} - \mathfrak{D} = 0 \\ nk - pl &= \mathfrak{D} - \mathfrak{D} = 0 \end{aligned} \tag{35}$$

The plane is uniquely fixed by the integers h,k and l called the **Miller indexes** of the plane. It is remarkable to note that the Laue equations can be rewritten in the explicit form as

$$\Delta\overrightarrow{k} = \overrightarrow{\mathbf{G}} \tag{36}$$

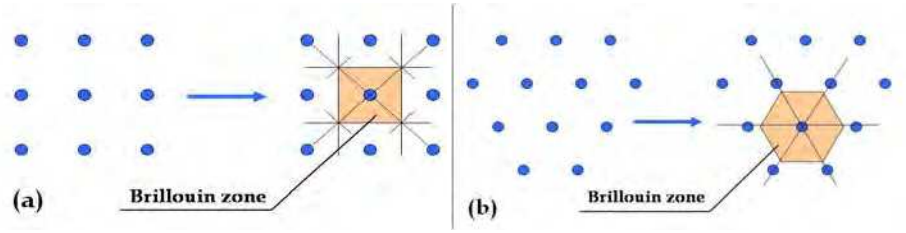

Fig. 5. a) First Brillouin Zone of a Square Lattice. b) First Brillouin Zone of a Hexagonal Lattice

the equation 36 is equivalent to the Bragg relation because the distance d from the plane with Miller indexes from the origin is equal to $\frac{2\pi}{|\vec{\mathbf{G}}|}$. So if $\vec{\mathbf{R}}$ ia a generic point of the lattice plane (hkl) we can say that

$$d = \frac{\vec{\mathbf{R}} \cdot \vec{\mathbf{G}}}{|\vec{\mathbf{G}}|} = \frac{2\pi}{|\vec{\mathbf{G}}|} \tag{37}$$

it follows that

$$|\Delta \vec{k}| = \frac{2\pi}{\lambda} 2\sin\theta = \frac{2\pi}{d}$$

$$2d\sin\theta = \lambda \tag{38}$$

where 2θ is the angle between the incident direction $\vec{k}$ and the diffracted direction $\vec{k'}$ and remembering that $\Delta \vec{k}$ is orthogonal to the plane, θ is also the incident angle of the plane itself. It is evident that the vector of the reciprocal lattice $n\vec{\mathbf{G}}$ shows the plane which is far from the origin of the value nd. For each lattice plane corresponds a constructive interference to the diffracted wave. It is more convenient to consider the *proximity cell* instead of the primitive cell. The Proximity Cell is the polyhedron whose faces lie on the plane which are orthogonal to the middle points of the lines who have the lattice point and its next one as extremes. The proximity cell of the reciprocal lattice is known as the First Brillouin Zone. By repeating the procedure with the further lattice point we can construct the second Brillouin Zone, the third and so on. Two of the most common lattice structures are the square lattice, whose first Brillouin zone we can see in Fig.5a and the hexagonal lattice whose first Brillouin zone is depicted in Fig.5b. Some points of high symmetry of these structures are very useful for the computation of the bandgap, as we will se further, and they are called the critical points.

8. Electromagnetic waves in the lattice and Bloch wave representation

We have showed a situation in which we used the so called Born (or single scattering) approximation where the lattice is weak point scatterer in a constant index. Background which is suitable to describe x-ray scattering. Now we move on to look at structures that are not point scatterers but high contrast dielectrics where bandgaps can occur. The field associated with the propagation of the electromagnetic waves is proportional to a vector $\vec{\mathbf{R}}$ of the direct lattice and to a variable σ which can vary on the degree of freedom of the field inside the primitive cell made by the translational vector. For a wave function, σ must be specified in the whole set of the points of the primitive cell and the field of the lattice vibrations has a number of degree

of freedom for each cell which is three times the number of the atom of each cell. The normal modes of the field $\xi(\sigma; \overrightarrow{\mathbf{R}})$ can be obtained as solutions of an eigenvalue problem as

$$\Omega\xi(\sigma; \overrightarrow{\mathbf{R}}) = \lambda\xi(\sigma; \overrightarrow{\mathbf{R}}) \tag{39}$$

where Ω is a linear operator, like the Hamiltonian. The allowed values for λ with the constraints are the eigenvalues of Ω with eigenfunctions $\xi(\sigma; \overrightarrow{\mathbf{R}})$. The translational symmetry can be described via a translational operator $\mathbb{T}(\overrightarrow{\mathbf{R}})$ defined as

$$\mathbb{T}(\overrightarrow{\mathbf{R_i}})\xi(\sigma; \overrightarrow{\mathbf{R}}) = \xi(\sigma; \overrightarrow{\mathbf{R}} + \overrightarrow{\mathbf{R_i}}) \tag{40}$$

It is important to remark that the vector $\overrightarrow{\mathbf{R}} + \overrightarrow{\mathbf{R_i}}$ is still a lattice vector. By applying twice the $\mathbb{T}$ operator we have

$$\mathbb{T}(\overrightarrow{\mathbf{R_2}})\mathbb{T}(\overrightarrow{\mathbf{R_1}})\xi(\sigma; \overrightarrow{\mathbf{R}}) = \mathbb{T}(\overrightarrow{\mathbf{R_2}})\xi(\sigma; \overrightarrow{\mathbf{R}} + \overrightarrow{\mathbf{R_1}}) = \tag{41}$$

$$\xi(\sigma; \overrightarrow{\mathbf{R}} + \overrightarrow{\mathbf{R_1}} + \overrightarrow{\mathbf{R_2}}) = \mathbb{T}(\overrightarrow{\mathbf{R_1}})\mathbb{T}(\overrightarrow{\mathbf{R_2}})\xi(\sigma; \overrightarrow{\mathbf{R}}) \tag{42}$$

so two translational operators commute. Let's consider the dynamic operator Ω. By the periodicity of the lattice every point of the lattice should be the same for the operator Ω, it means that

$$\mathbb{T}(\overrightarrow{\mathbf{R_i}})\Omega\xi(\sigma; \overrightarrow{\mathbf{R}}) = \Omega\mathbb{T}(\overrightarrow{\mathbf{R_i}})\xi(\sigma; \overrightarrow{\mathbf{R}}) \tag{43}$$

so for any ξ and for any $\mathbb{T}$, Ω commutes with all the $\mathbb{T}$ of the lattice. So we can find the eigenfunctions of 39 which are simultaneously eigenfunctions of the translational operators of the lattice. If $\xi(\sigma; \overrightarrow{\mathbf{R}})$ is an eigenfunction of Ω and $\mathbb{T}$ and $C(\overrightarrow{\mathbf{R_i}})$ is the eigenvalue of $\mathbb{T}(\overrightarrow{\mathbf{R_i}})$ so

$$\mathbb{T}(\overrightarrow{\mathbf{R_1}})\xi(\sigma; \overrightarrow{\mathbf{R}}) = \xi(\sigma; \overrightarrow{\mathbf{R}} + \overrightarrow{\mathbf{R_1}}) = C(\overrightarrow{\mathbf{R_1}})\xi(\sigma; \overrightarrow{\mathbf{R}}) \tag{44}$$

if we apply another translational operator $\mathbb{T}(\overrightarrow{\mathbf{R_2}})$

$$\mathbb{T}(\overrightarrow{\mathbf{R_2}})\mathbb{T}(\overrightarrow{\mathbf{R_1}})\xi(\sigma; \overrightarrow{\mathbf{R}}) = C(\overrightarrow{\mathbf{R_2}})C(\overrightarrow{\mathbf{R_1}})\xi(\sigma; \overrightarrow{\mathbf{R}}) \tag{45}$$

but the product $\mathbb{T}(\overrightarrow{\mathbf{R_2}})\mathbb{T}(\overrightarrow{\mathbf{R_1}})$ is equivalent to the translational operator $\mathbb{T}(\overrightarrow{\mathbf{R_2}} + \overrightarrow{\mathbf{R_1}})$

$$\mathbb{T}(\overrightarrow{\mathbf{R_2}} + \overrightarrow{\mathbf{R_1}})\xi(\sigma; \overrightarrow{\mathbf{R}}) = C(\overrightarrow{\mathbf{R_2}} + \overrightarrow{\mathbf{R_1}})\xi(\sigma; \overrightarrow{\mathbf{R}}) \tag{46}$$

and so we can deduce

$$C(\overrightarrow{\mathbf{R_2}} + \overrightarrow{\mathbf{R_1}}) = C(\overrightarrow{\mathbf{R_2}})C(\overrightarrow{\mathbf{R_1}}) \tag{47}$$

for any choice of the vector $\overrightarrow{\mathbf{R_1}}$ and $\overrightarrow{\mathbf{R_2}}$. Hence the eigenvalue C must have an exponential behavior in $\overrightarrow{\mathbf{R}}$:

$$C(\overrightarrow{\mathbf{R}}) = e^{\overrightarrow{\mu}\cdot\overrightarrow{\mathbf{R}}}\xi(\sigma, 0) \tag{48}$$

if the vector $\overrightarrow{\mu}$ would have real part different from zero, there should be directions in the infinite crystal in which the amplitude of the field would increase exponentially. In order to avoid that $\overrightarrow{\mu}$ must be of the form $i\overrightarrow{k}$ where $\overrightarrow{k}$ is a real vector. From this moment we will call $\xi(\sigma, 0)$ simply $\xi(\sigma)$, so the eigenfunctions of the dynamic problem must have the form of the well known Bloch Theorem:

$$\xi(\sigma; \overrightarrow{\mathbf{R}}) = \xi_{\overrightarrow{k}}(\sigma)e^{i\overrightarrow{k}\cdot\overrightarrow{\mathbf{R}}} \tag{49}$$

and the eigenfunctions of Ω are obtained by varying the vector $\overrightarrow{k}$ of the eigenvalue $exp(i\overrightarrow{k}\cdot\overrightarrow{\mathbf{R}})$ of the translational operator $\mathbb{T}(\overrightarrow{\mathbf{R}})$. Now the reciprocal lattice becomes useful, if the vector $\overrightarrow{k'}$ and $\overrightarrow{k}$ differ by a value of a translational vector of the reciprocal lattice $\overrightarrow{\mathbf{G}}$

$$\overrightarrow{k'} = \overrightarrow{k} + \overrightarrow{\mathbf{G}} \tag{50}$$

so remembering that $\overrightarrow{\mathbf{G}}\cdot\overrightarrow{\mathbf{R}} = 2n\pi$ where n is an integer, we can say

$$exp(i\overrightarrow{k'}\cdot\overrightarrow{\mathbf{R}}) = exp(\overrightarrow{\mathbf{G}}\cdot\overrightarrow{\mathbf{R}})exp(i\overrightarrow{k}\cdot\overrightarrow{\mathbf{R}}) = exp(i\overrightarrow{k}\cdot\overrightarrow{\mathbf{R}}) \tag{51}$$

so $\overrightarrow{k'}$ and $\overrightarrow{k}$ identify the same eigenvalue of the operator $\mathbb{T}(\overrightarrow{\mathbf{R}})$. The set of the solutions $\xi_{\overrightarrow{k}}$ of the dynamic problem is the same as the set of the solutions of $\xi_{\overrightarrow{k}+\overrightarrow{\mathbf{G}}}$. So without loss of generality we can focus our attention just on the primitive cell of the reciprocal lattice hence the **First Brillouin Zone**

9. Photonic band structures in the solid

A lot of results can be provided with the study of the simplest case; a periodic potential in one dimension V(x) so that

$$V(x) = V(x+a) \tag{52}$$

where a is the lattice constant. The Schrödinger Equation

$$-\frac{\hbar^2}{2m}\frac{d^2\psi}{dx^2} + V(x)\psi = E\psi \tag{53}$$

has two real, linear, independent solutions u(x) and v(x). Eq.52 implies that u(x+a) and v(x+a) are still solutions of the Schrödinger Equation, and so have to be linear combinations of u(x) and v(x);

$$u(x+a) = \alpha u(x) + \beta v(x)$$

$$v(x+a) = \gamma u(x) + \delta v(x) \tag{54}$$

with α, β, γ and δ real numbers. So it's useful to consider that in this case the Wronskian

$$\mathbf{W}(x) = v\frac{du}{dx} - u\frac{dv}{dx} = constant \tag{55}$$

independent from x, and this implies

$$\begin{aligned} W(x+a) = v(x+a)\frac{du(x+a)}{dx} - u(x+a)\frac{dv(x+a)}{dx} = \\ = (\alpha\delta - \beta\gamma)\{v\frac{du}{dx} - u\frac{dv}{dx}\} = \\ = (\alpha\delta - \beta\gamma)\mathbf{W}(x) \end{aligned} \tag{56}$$

so it means that

$$\alpha\delta - \beta\gamma = 1 \tag{57}$$

Let's consider now a generic solution of the Schrödinger Equation

$$\psi(x) = pu(x) + qv(x) \tag{58}$$

and let's call λ the value of ψ under translation operation a

$$\psi(x+a) = \lambda\psi(x) \tag{59}$$

so we can rewrite

$$pu(x+a) + qv(x+a) = \lambda(pu(x) + qv(x)) \tag{60}$$

the equation (54) implies that

$$\alpha p + \gamma q = \lambda p$$

$$\beta p + \delta q = \lambda q \tag{61}$$

which has a solution different from zero when

$$(\alpha - \lambda)(\delta - \lambda) - \beta\gamma = 0$$

$$\lambda^2 - (\alpha + \delta)\lambda + \alpha\delta - \beta\gamma = 0 \tag{62}$$

so finally just for the value of the equation

$$\lambda^2 - (\alpha + \delta)\lambda + 1 = 0 \tag{63}$$

which brings out two different cases: in the first one the two solutions λ_1 and λ_2 are real and different, and by $\lambda_1\lambda_2 = 1$ we have $\lambda_1 > 1$ and $\lambda_2 < 1$. If we translate ψ by a number of times n we have

$$\psi(x+na) = \lambda_1^n\psi(x) = \lambda_2^n\psi(x) \tag{64}$$

both solutions diverge, $\lambda_1^n\psi(x)$ for $x \to \infty$ and $\lambda_2^n\psi(x)$ for $x \to -\infty$. In the second case the two solutions are the complex conjugate of the other, and both module=1 so we can write

$$\lambda_1 = e^{ika}; \lambda_2 = e^{-ika} \tag{65}$$

in this case there is a degeneration of the eigenvalue of the energy. By the way it is useful to note the particular case in which both solutions are equal to 1 or -1. Because of equation 65 we can write

$$\psi(x+na) = e^{ikna}\lambda(x) \tag{66}$$

which is the Bloch theorem, and implies also that if we write $\psi(x)$ in the form

$$\psi(x) = u(k;x)e^{ikx} \tag{67}$$

so u is periodic both in the direct lattice

$$u(k;x+a) = u(k;x) \tag{68}$$

and the reciprocal one

$$u(k+\frac{2\pi}{a};x) = u(k;x) \tag{69}$$

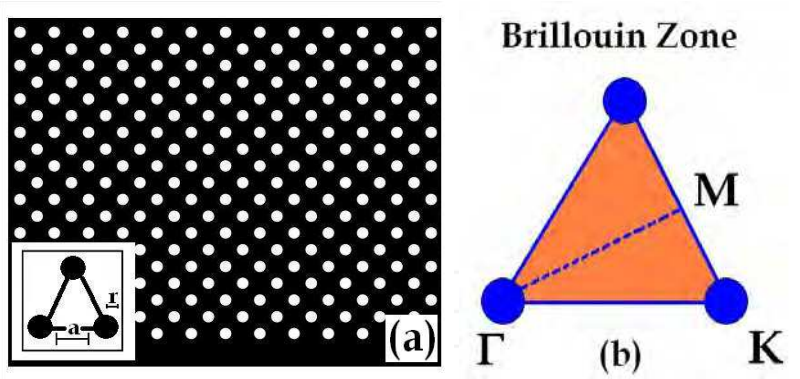

Fig. 6. a) two dimensional hexagonal array: (inset Primitive cell of the two dimensional hexagonal array showing lattice spacing *a* and radius *r*). b) First Brillouin Zone showing the critical points Γ, *K* and *M*

the physical solution allowed are the Bloch waves, so the plane waves modulated by a function which has the periodicity of the lattice. It is convenient to shrink *k* just to the First Brillouin Zone which is in this case the interval $[-\frac{\pi}{a}, \frac{\pi}{a}]$. The eigenvalue E(*k*) and E(-*k*) are degenerate and so E(*k*) is an even function of *k* which has also the periodicity of the reciprocal lattice.

$$E(k + \frac{2\pi}{a}) = E(k) \tag{70}$$

So if we want to perform a study of how the whole crystal propagates electromagnetic waves, it will be sufficient just to focus the study on the reciprocal lattice.

10. Two-dimensional hexagonal photonic crystal structure

Our aim is to fabricate a structure which will behave as resonant cavity for the single photon emission of the NV^- center. The best choice to pursue this goal would have been a $3D$ photonic crystal structure with a NV^- placed in its center, but unfortunately the fabrication of this kind of structure is challenging. So we decide to follow a different path using a quasi$-3D$ structure. In fact combining the photonic crystal feature and the total internal reflection (TIR), we obtain a structure which confines the light in the three directions XYZ. Indeed the light is confined by distributed Bragg reflection in the plane of periodicity (XY) and by total internal reflection in the perpendicular plane (Z), so we aim to fabricate a photonic crystal in a thin membrane. Let us start to consider the photonic crystal structure, as we have seen before, performing different choices of primitive cells gives rise to many different kind of structures, we have chosen a primitive cell which consists of an equilateral triangle of air holes, as seen in the inset of Fig.6(a). The repetition of the primitive cell gives rise a two dimensional hexagonal array, as shown in Fig.6(a). In Fig.6(b) we have shown the first brillouin zone for the two dimensional hexagonal lattice with its critical points. We decided to study this kind of structure because it is suitable for fabrication requirements and at the same time this photonic crystal structure has a bandgap tunable in the region of the desired wavelength with current fabrication technology. As previously discussed, in order to study the behavior of the whole crystal, we can just focus our attention on the primitive cell. The parameters of the primitive cell to take account of, are the radius of the holes **r**, and the lattice constant **a**,

namely the distance between holes centers. These two parameters allow to compute the whole behavior of the primitive cell and so of the photonic crystal which it makes. The first stage of the simulation process is to calculate the photonic band-gap of this structure, which gives a starting point for optimizing the lattice constants and hole radii. In order to compute the bandgap of the structure, we used a simulation software known as MIT Photonic-Bands (MPB) package, which is a free program for computing the band structures (dispersion relations) and electromagnetic modes of periodic dielectric structures, on both serial and parallel computers. It was developed by Johnson & Joannopoulos (2001) at MIT along with the Joannopoulos group. This program computes definite-frequency eigenstates (harmonic modes) of Maxwell's equations in periodic dielectric structures for arbitrary wavevectors, using fully-vectorial and three-dimensional methods. It is especially designed for the study of photonic crystals, but is also applicable to many other problems in optics, such as waveguides and resonator systems. (For example, it can solve for the modes of waveguides with arbitrary cross-sections). Remembering the first Brillouin zone depicted in Fig.6(b), if we imagine to wave vector k "moving" in a path assuming all the values from the critical point Γ through K and M and finally coming back to Γ, as also shown in the inset of Fig.7, we visualize the horizontal axis in the bandgap picture depicted in Fig.7. In that diagram we can appreciate how the behavior of the electromagnetic field inside the primitive cell responds to the variation of the frequency. So we can appreciate the first guided TE mode, the second guided TE mode and the bandgap between them, the yellow line, the values of the normalized frequency in that region gives us the range values for the lattice constant, in order to have a confinement for the desired wavelength.We performed many different simulations varying the ratio of the radius over the lattice constant, namely $\frac{\mathbf{r}}{\mathbf{a}}$ of the primitive cell, so we finally found the best choice, $\mathbf{r} = 0.30\mathbf{a}$ which gave us the widest bandgap for the triangular lattice. Now we take the middle value of the bandgap which gave us the value for $\frac{a}{\lambda}$**=0.375** giving the ratio for the computation of the lattice constant $a = 0.375\lambda$, where λ is the frequency of the light. So if we want to have a two-dimensional hexagonal photonic crystal structure which has a bandgap centered to wavelength of 637 nm, namely a PC structure resonant with the NV^- center emission, we have to use the values for lattice constant $a = 238.875$ nm and radius $r = 71.6625$ nm. Once we have a range for the values of the relevant parameters, we started to simulate the photonic crystal cavity made by a hexagonal array of air holes in diamond with three missing holes in the middle, also known as $L3$ cavity as shown in Fig.7b. In order to perform the simulations of the behavior of the cavity we used a Finite difference time domain (FDTD) software developed at University of Bristol by Professor Railton. In the FDTD method the time-dependent Maxwell's equations are discretized using central-difference approximations to the space and time partial derivatives the electric field vector components in a volume of space are solved at a given instant in time the magnetic field vector components in the same spatial volume are solved at the next instant in time the process is repeated over and over again until the desired transient or steady-state electromagnetic field behavior is fully evolved. In brief, the method involves dividing three-dimensional space into a grid of unit cells. Each cell is assigned six nodes, where the components of the electric and magnetic fields are stored. These values are updated at each time step by calculating the response to an incident field or excitation. The excitation takes the form of a Gaussian modulated sinusoid, as is appropriate for a dipole. A Fourier transform is taken on data sampled over time. The electric and magnetic fields ($\vec{E}$ and $\vec{H}$) at specific frequencies can be calculated at all points on the grid. The parameters that can be varied to optimize the performance of the cavity are the lattice constant, **a**, the radius of the air holes **r**. We performed many simulations changing the values of the lattice constant and

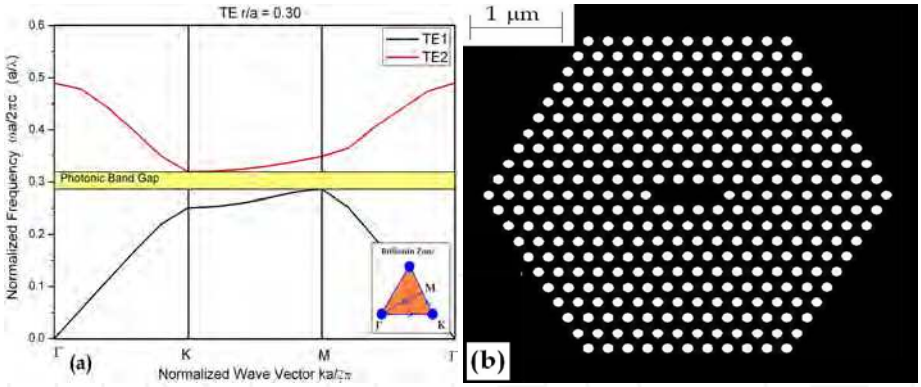

Fig. 7. a) Bandgap of the Hexagonal PC structure with the ratio r/a=0.3: Horizontal axis plots the normalized wavelength around the Brillouin zone going from $\Gamma - K - M - \Gamma$, Vertical axis shows normalized frequency $\frac{\omega a}{2\pi c} = \frac{a}{\lambda}$. b) L3 photonic crystal cavity structure

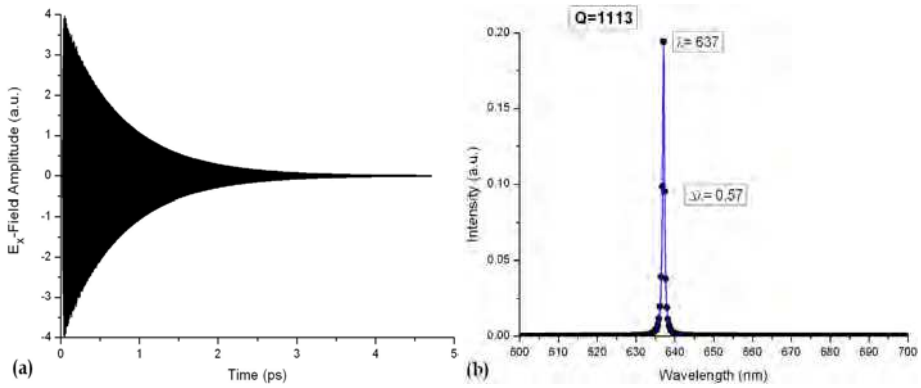

Fig. 8. a) Ring-down of the Ex component of the electromagnetic field inside the cavity. b) Fourier Transform of the Ex plot with Lorentzian Fit leading to an estimation of Q

the radius in the range gave by the bandgap calculation, in order to have a cavity resonant frequency of the NV^- emission. So we ended as results of the simulations with a L3 cavity resonant to a single mode frequency of $637nm$ with a small quality factor $Q = 1113$. In Fig.8(a) we can see the simulated ring down of the E_x component of the electromagnetic field inside the L3 cavity, in Fig.8(b) is shown its Fourier Transform with a Lorentzian fit which allowed us to calculate the resonant frequency, $\lambda = 637nm$ and the Full Half Width Maximum (FHWM) $\Delta\lambda = 0.57$. We checked in a large range surrounding the resonant frequency considering many different values but this left the value of quality factor unchanged, so we decided for clarity purposes to show a small range surrounding the resonant frequency. In this early we chose a cavity thickness of 500 nm which was not optimum The second step consisted of the calculation of the thickness of the membrane, in the direction perpendicular to the photonic crystal structure the field is confined by total internal reflection (TIR) by creating a suspended membrane. To ensure single-mode operation at wavelength $\lambda = 637nm$, a slab thickness of $\sim \lambda/4n$ is required as discussed by Joannopoulous et al. (1995). So we simulated the behavior

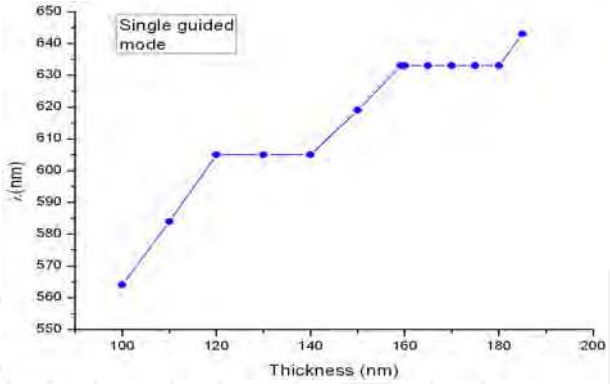

Fig. 9. Wavelength of the confined single mode emission in the membrane respect to the variation of its thickness

of the light from a source placed in the center of a membrane with a photonic crystal L3 cavity for different thickness of the membrane. As we can see in in Fig.9, where it is plot the change of the wavelength of the confined single mode with respect to the thickness of the membrane. The plot shows the expected blue-shift as we thin the membrane. We can correct for this shift by scaling all dimensions after optimizing the Q-Factor. In order to increase Q-factor of the light inside the cavity having a small modal volume, Akahane et al. (2003) demonstrated that the light should be confined gently in order to reduce scattering into leaky modes. The strategy to obtain gentler confinement is to change the condition for Bragg reflection at the cavity edge. We changed the radii of the holes at the side of to the cavity and eventually we shifted the holes at the end to the cavity. So first we varied the size of the holes in the first lines next to the cavity, as shown in the inset of Fig.10, modifying the geometry of the lattice structure surrounding the defect, following the idea proposed by Zhang & Qiu (2004). We improved so far the value of the simulated quality factor, as shown in Fig.10, where it is plot the behavior of simulated quality factor as function of the radius of the holes in the first lines next to the cavity. We note that a value for the small radius $R_1 = 0.198a$ gives the highest value for the quality factor. After that modification we performed a further modification in which we aim to gently confine the mode at the edge of the activity by shifting the nearest holes as we can see in the inset of Fig.11. So if we shift the position of the air holes at the edge we change the reflection conditions, but on the other way round the light penetrates more inside the mirror and is reflected perfectly. In Fig.11 we have plot the behavior of the simulated quality factor as function of the shift of the nearest holes, and we can clearly see that there is a peak for $d = 0.11a$, which is the value of the distance at which we shift the holes. Choosing a thickness of 185 nm we now optimize the Q-factor as shown in Fig.12a where we plot the behavior of the Quality factor respect to change of the thickness. We can see clearly that it is highest for $thickness = 185nm$ which is the value we have chosen for the next steps. The quality factor, Q, can be separated into the in-plane value, $Q_{\parallel}$, and a vertical value, $Q_{\perp}$. $Q_{\parallel}$ can, in principle, be made arbitrarily high by increasing the number of periods. The cavity is surrounded by 14 periods in all directions. Simulation results showed that increasing the number of periods to 25 changes the quality factor by less than 2%. This means that the total Q approaches $Q_{\perp}$ as described also by Tomljenovic-Hanic et al. (2006). Finally in order to increase the quality factor with a small modal volume we decided to keep 14 periods surrounding the

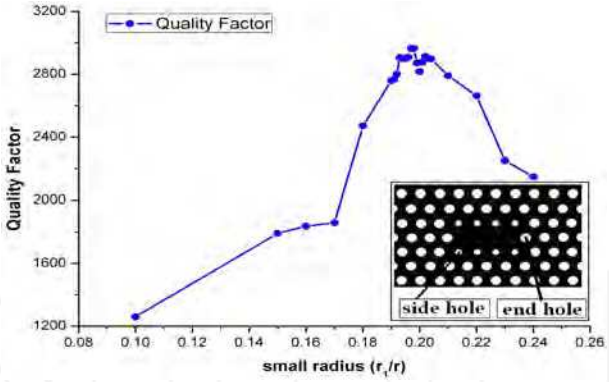

Fig. 10. Quality factor as function of the radius of the nearest holes of the $L3$ cavity. Inset:schematic diamagram of the $L3$ cavity modified with different value for the holes in the first lines next to the cavity

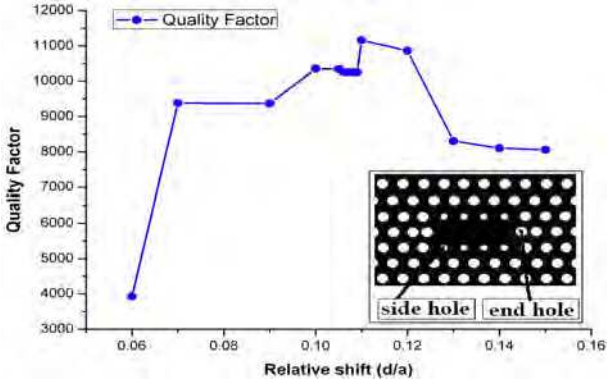

Fig. 11. Quality factor as function of the shift of the nearest holes of the $L3$ cavity. Inset:schematic diamagram of the $L3$ cavity modified with different value for the holes in the first lines next to the cavity

cavity, because we did not want to have too many holes for fabrication purposes, the final structure perfectly optimized is shown in Fig.12b. In Fig.13 we plot the intensity ($|E^2|$) of the electromagnetic field, higher in red, lower in blue, from top view ($x-y$ plane)Fig.13a and side view ($z-y$ plane)Fig.13b respectively. Clearly we see that the light is confined by distributed Bragg reflection in the plane of periodicity (xy) and by total internal reflection in the perpendicular plane (z). The result of increasing the total size of the photonic crystal is that we achieve a highest quality factor $Q \simeq 32.000$. This value we simulated agrees with the best values reached by other groups like Tomljenovic-Hanic et al. (2009). We show the time decay and the fourier transform in Fig.14. In order to verify that the photonic crystal cavity produce an enhancement of the Purcell factor of the NV^-center we need also to calculate the modal volume of the cavity. The modal volume, defined by Coccioli et al. (1998) is

$$V_{eff} = \frac{\int \epsilon(r)|E(r)|^2 d^3r}{[\epsilon(r)|E(r)|^2]_{max}} \tag{71}$$

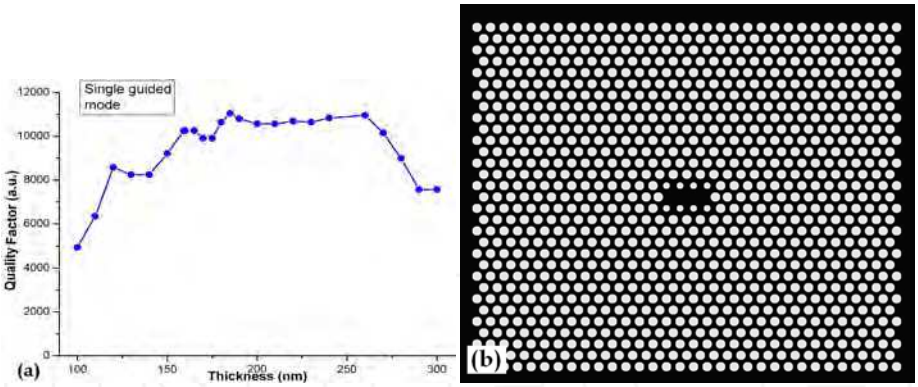

Fig. 12. a)Quality factor for the confined single mode emission in the membrane according to the variation of its thickness, b)$L3$ photonic crystal cavity structure modified with smaller radius and nearest holes shifted

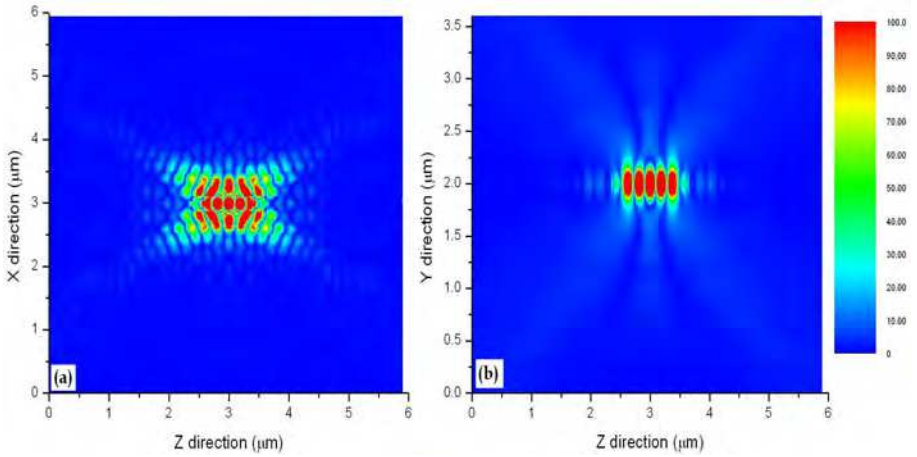

Fig. 13. a) Plot of the intensity of electromagnetic field confined by the photonic crystal bandgap cavity,(top view of $x-z$ plane). b) Plot of the intensity of electromagnetic field confined by total internal reflection, (top view of $y-z$ plane). higher intensity in red lower in blue)

where $\epsilon(r)$ is the dielectric constant and $|E(r)|^2$ is the electric field intensity at position r and the integral is normalized by the maximum intensity in the cavity. In order to estimate V_{eff} we used a procedure shown in Ho et al. (2011) which creates different frequency snapshots at different position in the computational grid during the simulation, recording all the information of the electromagnetic field in each slice. Using this method and the structure depicted in Fig.12 we estimate the modal volume of the field inside the photonic crystal to be $V_{eff} = 0.0162\mu m^3$ which is a value close to the one we assumed on our work on non-demolition measurement, described in Young et al. (2009), and is also consistent with results obtained by other groups as for example Tomljenovic-Hanic et al. (2009). The modal volume can be normalized to the cubic wavelength of the resonant mode $(\frac{\lambda}{n})^3$ in a medium

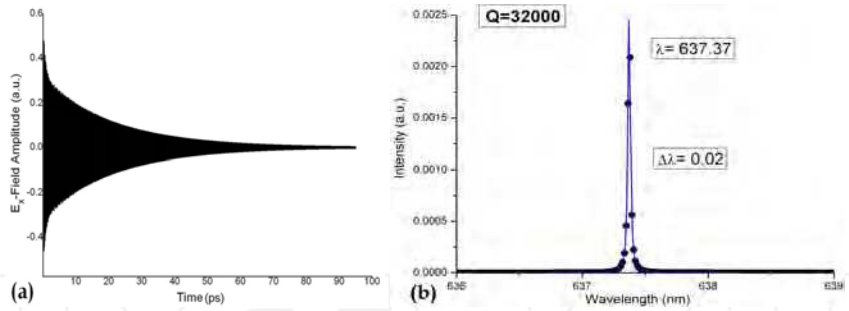

Fig. 14. a) Ringdown of the E_x component of the electromagnetic field inside the optimized cavity. b) Fourier Transform of the E_x plot with Lorentzian Fit leading to an estimation of Q=32000

of refractive index (n) defined as:

$$V_{opt} = \frac{V_{eff}}{(\lambda/n)^3} \tag{72}$$

So for our case the value of the normalized volume for a the wavelength of the NV^- center ($\lambda = 637$ nm) in the diamond which has refractive index $n = 2.4$ corresponds to

$$V_{opt} = 0.8665(\frac{\lambda}{n})^3. \tag{73}$$

Remembering the Purcell factor, as described in Fox (2006),

$$F_P = \frac{3Q\lambda^3}{4\pi^2 n^3 V_{eff}} \tag{74}$$

we can estimate the enhancement of spontaneous emission rate of the NV^- center inside the photonic crystal cavity

$$F_p = 2.8 \times 10^3. \tag{75}$$

Remembering the definition of the coupling rate and radiative decay (Fox (2006)) we can see that in this case $g_0/2\pi = 11.7028$ GHZ, with a radiative decay rate $\kappa/2\pi = 14.7174$ GHZ. The NV^- center usually has a typical emission lifetime $\tau = 12$ ns which gives us a rate $\gamma/2\pi = 1/\tau = 0.0833$ GHZ. Finally we can compare these three main parameters, g_0, κ and γ, in order to reach the strong-coupling regime the coherent coupling g_0 between the transition and the cavity field has to exceed the decay rates of the color center γ and the cavity κ, obeying $4g_0 > (\kappa + \gamma)$. In this particular case we can estimate $4g_0/(\kappa + \gamma) > 3.16$, which tells us that we would be in the strong coupling regime.

11. Fabricating photonic crystals using focus ion beam etching

Having simulated photonic crystal structure cavities we have begun fabrication via focused ion beam etching (FIB). Our aim is to create a suspended membrane with the “Noda" cavity previously described. In the first fabrication step, the diamond crystal is undercut by turning side-on and etching to obtain a $200nm$ thick slab attached to the bulk (a suspended slab). We needed to etch the membrane first, because if we have done the photonic crystal structure first, at the stage in which we etch the membrane some sputtering could have filled the

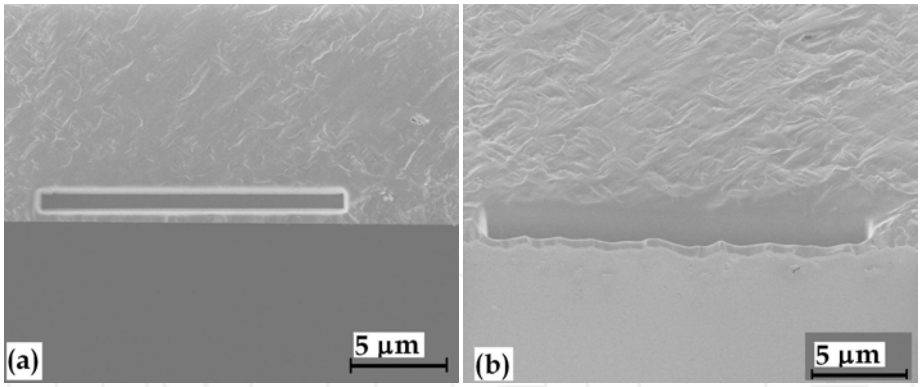

Fig. 15. secondary electron image of a etched membrane in the diamond sample. a) a top view of the etched membrane, b) 45° Tilted view of the etched membrane

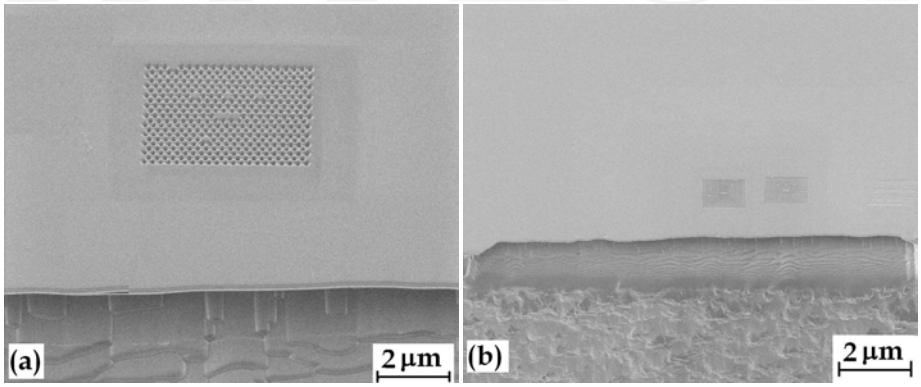

Fig. 16. a) Tilted view of the L3 cavity taken with FIB at different tilt and magnitude. b) larger image of the membrane and the cavities

holes. In order to etch the membrane we mounted the sample on a stage, and then titled it to 90° and after we covered the implanted NV^-center array zone with silver, in order to protect the implanted NV^-s, we etched a thin membrane of 200nm according to the results of the simulation previously shown. In Fig.15(a) we can see a top view of the membrane and in Fig.15(b) we can see an image of the same membrane tilted by 45°. After we made the membrane we repositioned the sample horizontally and finally we etched the hexagonal air hole array with cavity formed from three filled holes. Fig.16 shows two views, tilted of 45° at different magnifications of the resulting structure. Both were secondary electron images taken with FIB after the etching. In Fig.16(a), we can see the photonic crystal cavity and etched in the membrane which is more evident in Fig.16(b) where we have a scan over a larger area which shows the size of the cavities compared to the suspended membrane. In the top view, shown in Fig.17(a), we can observe the cavity and notice some imperfections in it due to the FIB technique which creates deposit of etched material during the scanning. In Fig.17(b) we can see an image taken with a confocal microscope,in which blue color means low intensity and red color means high intensity. Fig.17(b) is remarkable because we can clearly

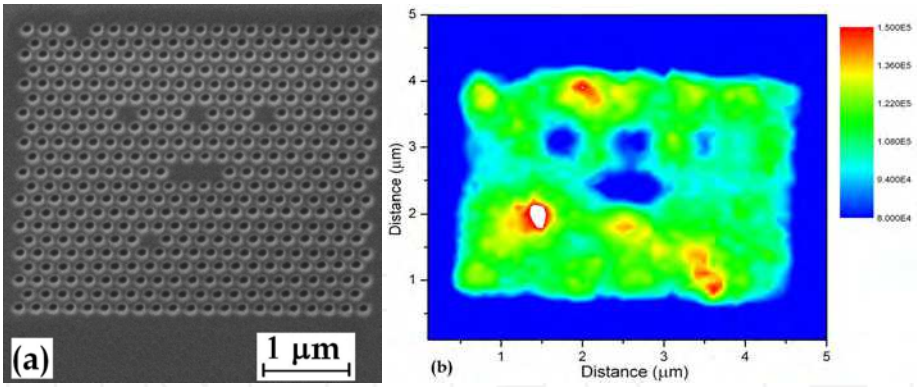

Fig. 17. a) Secondary electron emission image of the top view of the L3 cavity. b) Fluorescence image taken with the confocal microscope (color red: high intensity, color blue:low intensity).

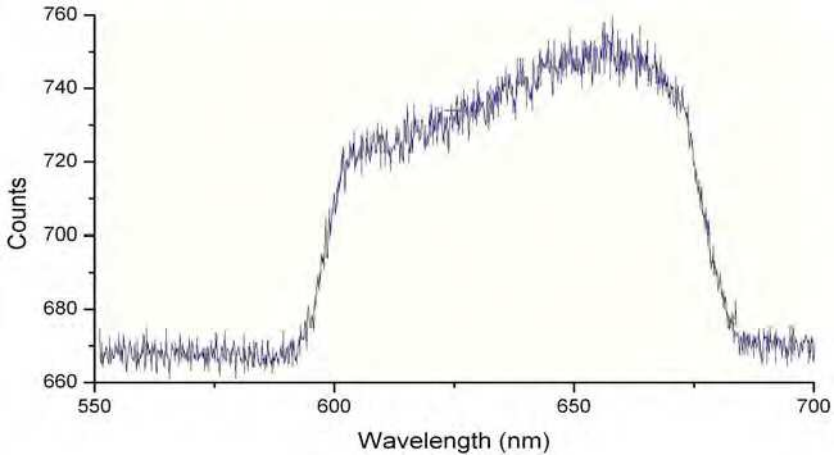

Fig. 18. Image of the emission spectrum taken at the center of the photonic crystal cavity. No narrow peaks are seen as would be expected from cavity resonance effects.

see reduced fluorescence in the un-etched zone, forming the cavity. Because there is no (or less) etch damage in these regions. This is an encouraging result because it means that if there were a NV^- center in the cavity we might be able to see it. We performed some measurement of the spectrum of the light emitted from the cavity region. Unfortunately we were not able to see any enhancement of the signal as we might expect from a cavity resonance, but just a broad emission as shown in Fig.18. At this stage we decided to make a step back and to perform a preliminary study about the real possibility of coupling a single NV^- center to a larger structure etched in the diamond with FIB.

12. Conclusion

In this work we discussed about the feasibility of NV^- centers as single photon emitters and how to use its spin as qubit for quantum computing applications, remarking the many

advantages that the use of NV^- center in diamond would produce. One of the key challenges in order to perform a real implementation of a quantum computer concerns the possibility of handling the qubit. The spin of the ground state of the NV^- center shows some characteristics we have described earlier in this work, which looks very promising for this purposes. One of the crucial step in order to perform spin readout and non demolition measurement of the spin of the NV^- center is represented by increasing the coupling between the light and the solid state system. We showed a way to increase the coupling between the NV^- and the light by placing the NV^- center in a photonic crystal cavity. We characterized the photonic crystal cavity tuning it to be resonant with the NV^- center emission, having had encouraging results in the simulation and fabrication of the cavity, in that we reached a reasonable high value of quality factor and small modal volume. Another very important aspect in order to build a quantum computer is represented by the possibility of handling a single photon source. In order to use NV^- as single photon emitter, one of the challenges is represented by the light collection. We developed in order to increase the light collection from the NV^- center by etching a solid immersion lens around it, proposing a technique (Marseglia et al. (2011)) in order to locate NV^- centers with accuracy of $10nm$, and fabricate structure around them. In future works we will use the technique we have recently developed, in order to create a photonic crystal around a single NV^- center. Another important path we want to follow consist in exploiting another useful color center in the diamond, the chromium center. This center acts as a single photon emitter as well but with a narrower spectrum. It has a resonant wavelength of $755nm$ which is in the wavelength range for the si photon counting detector, allowing us to detect them with high efficiency. We are very interested in using the technique we have developed in order to etch photonic crystal around single chromium center and coupling with it, this would allow us to increase the light collection from the chromium center permitting it to be used as an ultra bright single photon emitter. As it emits at $755nm$ it is compatible with integrated photonic circuits being developed in our group by Politi et al. (2008). Similarly the nickel-nitrogen complex (NE8) center in diamonds, studied by Gaebel et al. (2004); Rabeau et al. (2005), has narrow emission bandwidth of $1.2nm$ at room temperature with emission wavelength around $800nm$, again suitable for Si detectors and quantum photonic circuits. In addition, in this spectral region little background light from the diamond bulk material is detected, which made it an interesting possible candidate for single photon source. Once we are able to locate an $NE8$ (or other suitable narrowband) center we will extend the registration procedure developed to allow fabrication of photonic crystal structure around individual defects, ending in the measurement of Q-factors and Purcell enhanced emission. In order to handle and guide the light emitted from the source a detailed study of parameters of a photonic crystal waveguide in the diamond will be required as demonstarted by Song et al. (2007). We will simulate the behavior of the electromagnetic field inside the cavity and how it will couple with the waveguide. A good response will lead us to fabricate and then measure the effective coupling. We will also explore different etching techniques such as Reactive-Ion Etching (RIE) which will allow us to create membranes and very thin structures in diamond with a high precision. This will be useful in order to create different structures around registered NV^- centers, for instance with photonic crystal nanobeam cavities studied by Deotare et al. (2009). This kind of structures as the remarkable advantage to be very easy to fabricate offering a huge quality factor and a very small modal volume.

13. References

Akahane, Y., Asano, T., Song, B.-S. & Noda, S. (2003). High-q photonic nanocavity in a two-dimensional photonic crystal, *Nature* 425: 944.

Coccioli, R., Borodsky, M., Kim, K. W., Rahmat-Samii, Y. & Yablonovitch, E. (1998). Smallest possible electromagnetic mode volume in a dielectric cavity, *IEE Proc.-Optoelectron.* 145: 391–397.

Deotare, P. B., McCutcheon, M. W., Frank, I. W., Khan, M. & Loncar, M. (2009). Coupled photonic crystal nanobeam cavities, *Appl. Phys. Lett.* 95: 031102.

Fox, M. (2006). *Quantum Optics*, 2 edn, Oxford University Press.

Gabel, T., Dohman, M., Popa, I., Wittmann, C., Neumann, P., Jelezko, F., Rabeau, J. R., Stavrias, N., Greentree, A. D., Prawer, S., Meijer, J., Twamley, J., Hemmer, P. R. & Wrachtrup, J. (2006). Room-temperature coherent coupling of single spins in diamond, *Nature Physics* 2: 408 – 413.

Gaebel, T., Popa, I., Gruber, A., Domhan, M., Jelezko, F. & Wrachtrup, J. (2004). Stable single-photon source in the near infrared, *New Journal of Physics* 6: 98.

Gali, A., Fyta, M. & Kaxiras, E. (2008). Ab initio supercell calculations on nitrogen-vacancy center in diamond: Electronic structure and hyperfine tensors, *Physical Review B* 77: 155206.

Gruber, A., Dräbenstedt, A., Tietz, C., Fleury, L., Wrachtrup, J. & von Borczyskowski, C. (1997). Scanning confocal optical microscopy and magnetic resonance on single defect centers, *Science* 276.

Hanson, R., Mendoza, F. M., Epstein, R. J. & Awschalom, D. D. (2006). Polarization and readout of coupled single spins in diamond, *Phys. Rev. Lett.* 97: 087601.

Ho, Y.-L. D., Ivanov, P. S., Engin, E., Nicol, M., Taverne, M. P. C., HU, C., Cryan, M. J., Craddock, I. J., Railton, C. J. & Rarity, J. G. (2011). Three-dimensional fdtd simulation of inverse three-dimensional face-centered cubic photonic crystal cavities, *IEEE J. Quantum Electron.* in press.

Jelezko, F., Gaebel, T., Popa, I., Gruber, A. & Wrachtrup, J. (2004a). Observation of coherent oscillation of a single nuclear spin and realization of a two-qubit conditional quantum gate, *Phys. Rev. Lett.* 93: 7.

Jelezko, F., Gaebel, T., Popa, I., Gruber, A. & Wrachtrup, J. (2004b). Observation of coherent oscillations in a single electron spin, *Phys. Rev. Lett.* 92: 7.

Jelezko, F. & Wrachtrup, J. (2004). Read-out of single spins by optical spectroscopy, *J. Phys.: Condens. Matter* 16: 104.

Joannopoulous, J. D., Meade, R. D. & Winn, J. N. (1995). *Photonic crystals: Molding the flow of light*, Princeton University Press.

Johnson, S. G. & Joannopoulos, J. D. (2001). Block-iterative frequency-domain methods for maxwell's equations in a planewave basis, *Optics Express* 8: 173.

Kurtsiefer, C., Mayer, S., Zarda, P. & Weinfurter, H. (2000). Stable solid-state source of single photons, *Phys. Rev. Lett.* 85: 290.

Manson, N. B., Harrison, J. P. & Sellars, M. J. (2006). Nitrogen-vacancy center in diamond: Model of the electronic structure and associated dynamics, *Phys. Rev. B* 74: 104303.

Marseglia, L., Hadden, J. P., Stanley-Clarke, A. C., Harrison, J. P., Patton, B., Ho, Y.-L. D., Naydenov, B., Jelezko, F., Meijer, J., Dolan, P. R., Smith, J. M., Rarity, J. G. & O'Brien, J. L. (2011). Nano-fabricated solid immersion lenses registered to single emitters in diamond, *Appl. Phys. Lett.* 98: 133107.

Neumann, P., Mizuochi, N., Rempp, F., Hemmer, P., Watanabe, H., Yamasaki, S., Jacques, V., Gaebel, T., Jelezko, F. & Wrachtrup, J. (2008). Multipartite entanglement among single spins in diamond, *Science* 320: 1326.

Politi, A., Cryan, M. J., Rarity, J. G., Yu, S. & O'Brien, J. L. (2008). Silica-on-silicon waveguide quantum circuits, *Science* 320: 646–649.

Rabeau, J. R., Chin, Y. L., Prawer, S., Jelezko, F., Gaebel, T., & Wrachtrup, J. (2005). Fabrication of single nickel-nitrogen defects in diamond by chemical vapor deposition, *Appl. Phys. Lett.* 86: 131926.

Song, B.-S., Noda, S. & Asano, T. (2007). Photonic devices based on in-plane hetero photonic crystals, *Science* 300: 1537.

Su, C. H., Greentree, A. D. & Hollenberg, L. C. L. (2008). Towards a picosecond transform-limited nitrogen-vacancy based single photon source, *Optics Express* 16: 6240.

Tamarat, P., Manson, N. B., Harrison, J. P., McMurtrie, R. L., Nizovtsev, A., Santori, C., Beausoleil, R. G., Neumann, P., Gaebel, T., Jelezko, F., Hemmer, P. & Wrachtrup, J. (2008). Spin-flip and spin-conserving optical transitions of the nitrogen-vacancy centre in diamond, *New Journal of Physics* 10: 045004.

Tomljenovic-Hanic, S., Greentree, A. D., de Sterke, C. M. & Prawer, S. (2009). Flexible design of ultrahigh-q microcavities in diamond-based photonic crystal slabs, *Optics Express* 17: 6465.

Tomljenovic-Hanic, S., Steel, M. J., de Sterke, C. M. & Salzman, J. (2006). Diamond based photonic crystal microcavities, *Optics Express* 14: 3556.

van Oortt, E., Manson, N. B. & Glasbeekt, M. (1988). Optically detected spin coherence of the diamond n-v centre in its triplet ground state, *J. Phys. C: Solid State Phys.* 21: 4385–4391.

Wang, C. F., Hanson, R., Awschalom, D. D., Hu, E. L., Feygelson, T., Yang, J. & Butler, J. E. (2007). Fabrication and charcterization of two-dimensional photonic crystal microcavities in nanocrystalline diamond, *Appl.Phys.Lett.* 91: 201112.

Young, A., Hu, C. Y., Marseglia, L., Harrison, J. P., O'Brien, J. L. & Rarity, J. G. (2009). Cavity enhanced spin measurement of the ground state spin of an nv center in diamond, *New Journal of Physics* 11: 013007.

Zhang, Z. & Qiu, M. (2004). Small-volume waveguide-section high q microcavities in 2d photonic crystal slabs, *Optics Express* 12: 3988–3995.

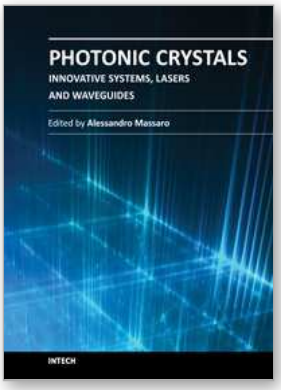

Photonic Crystals - Innovative Systems, Lasers and Waveguides

Edited by Dr. Alessandro Massaro

ISBN 978-953-51-0416-2
Hard cover, 348 pages
Publisher InTech
Published online 30, March, 2012
Published in print edition March, 2012

The second volume of the book concerns the characterization approach of photonic crystals, photonic crystal lasers, photonic crystal waveguides and plasmonics including the introduction of innovative systems and materials. Photonic crystal materials promises to enable all-optical computer circuits and could also be used to make ultra low-power light sources. Researchers have studied lasers from microscopic cavities in photonic crystals that act as reflectors to intensify the collisions between photons and atoms that lead to lazing, but these lasers have been optically-pumped, meaning they are driven by other lasers. Moreover, the physical principles behind the phenomenon of slow light in photonic crystal waveguides, as well as their practical limitations, are discussed. This includes the nature of slow light propagation, its bandwidth limitation, coupling of modes and particular kind terminating photonic crystals with metal surfaces allowing to propagate in surface plasmon-polariton waves. The goal of the second volume is to provide an overview about the listed issues.

How to reference

In order to correctly reference this scholarly work, feel free to copy and paste the following:

Luca Marseglia (2012). Photonic Crystal Coupled to N-V Center in Diamond, Photonic Crystals - Innovative Systems, Lasers and Waveguides, Dr. Alessandro Massaro (Ed.), ISBN: 978-953-51-0416-2, InTech, Available from: http://www.intechopen.com/books/photonic-crystals-innovative-systems-lasers-and-waveguides/photonic-crystal-coupled-to-n-v-center-in-diamond

INTECH
open science | open minds

InTech Europe
University Campus STeP Ri
Slavka Krautzeka 83/A
51000 Rijeka, Croatia
Phone: +385 (51) 770 447
Fax: +385 (51) 686 166
www.intechopen.com

InTech China
Unit 405, Office Block, Hotel Equatorial Shanghai
No.65, Yan An Road (West), Shanghai, 200040, China
中国上海市延安西路65号上海国际贵都大饭店办公楼405单元
Phone: +86-21-62489820
Fax: +86-21-62489821